Available online at www.sciencedirect.com

SciVerse ScienceDirect

Ceramics International 39 (2013) 1241–1247

CERAMICS INTERNATIONAL

www.elsevier.com/locate/ceramint

Far infrared and microstructural studies of mechanically activated nickel manganite

S.M. Savić[a,*], M.V. Nikolić[a], K.M. Paraskevopoulos[b], T.T. Zorba[b], N. Nikolić[a], V. Blagojević[c], O.S. Aleksić[a], G. Branković[a]

[a]*Institute for Multidisciplinary Research, University of Belgrade, Kneza Višeslava 1, 11030 Belgrade, Serbia*
[b]*Physics Department, Solid State Section, Aristotle University of Thessaloniki, 54124 Thessaloniki, Greece*
[c]*Faculty of Electrical Engineering, University of Belgrade, Bulevar kralja Aleksandra 73, 11000 Belgrade, Serbia*

Received 22 June 2012; received in revised form 17 July 2012; accepted 17 July 2012
Available online 24 July 2012

Abstract

Nickel manganite powder synthesized by calcination of a stoichiometric mixture of manganese (MnO Aldrich 99.9%) and nickel oxide (NiO Merck, 99.5%) containing 0.5 wt% CoO and Fe_2O_3, was additionally mechanically activated in a high energy planetary ball mill for 5–60 min. The resulting powders were uniaxially pressed into disc shape pellets and then sintered for 60 min at 900 °C, 1050 °C and 1200 °C. Morphological changes of the obtained nickel manganite ceramics induced by mechanical activation were monitored using scanning electron microscopy, while changes in structural characteristics were followed using X-ray powder diffraction. Room temperature far infrared reflectivity spectra for all sintered samples were recorded in the frequency range between 50 $cm^{-1}$and 1200 cm^{-1}. The observed spectra for all samples showed the presence of the same oscillators, but their intensities depended on the sintering temperature and the time of mechanical acivation. Transversal and longitudinal optical modes were calculated for six ionic oscillators (four strong, and two shoulders) belonging to the nickel manganite partially inverse spinel structure.

Keywords: A. Powders: solid state reaction; B. Electron microscopy; C. Optical properties

1. Introduction

The main characteristic of thermistors with a negative temperature coefficient is an exponential decrease in specific resistivity (ρ) over a wide temperature range. NTC thermistors have found widespread use for different (multiple) applications, such as temperature and pressure sensing, device protection, time delay circuits, voltage regulation, fire wire sensors [1–4], infrared detectors [5,6], fluid flow [7] and microflow sensors [8,9], miniature chip sensors [10].These materials are used in many applications (domestic and industrial) either to sense or to respond to changes in temperature.

NTC ceramics have been used as a material for thermistor devices for a long time. Since S. Ruben discovered the first pyrometer device in 1930 until nowadays, exploration of materials with this type of behavior (resistivity falls with temperature) was and remains very inspirational. For electroceramics industry and manufacturers, one of the main segments is investigation and development of NTC ceramic thermistors. NTC ceramics, based on transitional metal oxides have found widespread use in electronics [11,4,12]. Recently, much work has been done in the field of thin NTC films and microbolometer applications [13,14].

Nickel manganite as a negative temperature coefficient material is often used in industrial and domestic applications where cost efficient but reliable temperature sensing is required. It can be prepared by the commonly used solid state reaction [15,16], milling with mixed oxalates [17,18] or chemically from different precursors [12,19]. It has a cubic spinel structure and the spinel type is intermediate. Part of Ni^{2+} cations (which have a strong preference for octahedral sites) are relocated from tetrahedral to octahedral intersticies and this occupation induces the appearance of $Mn^{3+/4+}$ redox couples. Mn^{3+} ions in octahedral sites disproportionate

*Corresponding author. Tel.: +381112085032.
E-mail address: slavicas@imsi.rs (S.M. Savić).

0272-8842/$ - see front matter © 2012 Elsevier Ltd and Techna Group S.r.l. All rights reserved.
http://dx.doi.org/10.1016/j.ceramint.2012.07.054

to Mn^{2+} and Mn^{4+} and Mn^{2+} ions move to tetrahedral sites to compensate Ni^{2+} vacancies and cation arrangement is: $Mn^{2+}[Ni_x^{2+}Mn_x^{4+}Mn_{2-2x}^{3+}]O_4^{2-}$.

The well known thermally activated hopping mechanism between Mn^{3+} and Mn^{4+} placed in octahedral sites is responsible for conduction. Electrical conductivity, as well as change of resistivity, caused by jumping electrons from Mn^{3+} to Mn^{4+} ions, placed in the octahedral sites of spinel are determined by cations distribution between A and B sites of the spinel.

The cation inverse parameter x has an influence on all physical properties and it determines both electrical [11,20,21] as well as magnetic properties. Due to the fact that nickel manganite is a ferrimagnetic material, its magnetic properties were also investigated [12,22–26]. Our previous work was based on investigations of electric and electronic transport properties of nickel manganite [27–29] but it also included an analysis of optical properties [30,31].

In our recent work [32], we observed electrical and microstructural changes in nickel manganite powder during mechanical activation. In this case we also combined solid state and mechanical activation reaction of the powder, knowing the fact that mechanical activation is a powerful tool and what it brings to a system. Having all this in mind, the aim of this paper is to illuminate a little better optical properties of this material and make a correlation with synthesis parameters (time of mechanical activation and sintering temperature). Optical reflectivity as a function of the wave number of nickel manganite ceramics sintered at different temperatures (prepared from powders mechanically activated for different times) were recorded in infrared and far infrared range and later numerically analyzed.

2. Experimental

A stoichiometry mixture of starting manganese and nickel oxide was calcinated for 1 h at 1050 °C and then, the powder was additionally mechanically activated in a high energy Fritsch Pulverisette 5 planetary ball mill. Mechanical activation was performed in a continual regime using Fe balls with the constant disc rotation speed of 400 rpm and ball- to-powder ratio 10:1 and the milling time (t) was 5, 15, 30, 45 and 60 min. The as-prepared powders were pressed with 196 MPa into disc-shaped pellets 10 mm in diameter and then sintered in air using a Lenton LT 818 furnace with a constant heating rate of 15 °C/min from room temperature to 900 °C, 1050 °C and 1200 °C and then held for 60 min. The corresponding samples are labeled as NMO-s-T-t.

X-ray analysis was conducted on a Seifert ID 3000 X-ray diffractometer with CuK_α radiation and a step scan mode of 0.05°/10 s. Le-Bail full pattern profile fitting was used to calculate unit cell parameters.

Microstructural characterization of sintered, fractured and thermally etched samples was carried out on Vega TS 5130MM and JEOL JSM 6400 LV scanning electron microscopes.

Room temperature far infrared optical reflectivity measurements were performed on a Bruker 113V FTIR spectrometer using normal incidence light in the range between 100 cm^{-1} and 1200 cm^{-1}. Prior to measuring the samples were highly polished with P1000 and P1500 sandpaper.

3. Results and discussion

X-ray diffraction analysis showed that all analyzed samples samples contained a single-phase spinel structure, with a very slight change in lattice parameter. Confirmation of the existence of single phase $NiMn_2O_4$ is depicted on Fig. 1. showing X-ray diffractogram of the sample additionally activated 15 min and then sintered at 1200 °C for 60 min. Values of the determined structural parameters for nickel manganite samples sintered at 1200 °C mechanically activated for different times are given in Table 1. Analysis of the determined values shows that the lattice parameter values are very similar for all analyzed $NiMn_2O_4$ samples regardless of the activation time. The value of the lattice constant for a sample activated for 30 min sintered at 1050 °C was lower than values obtained for samples sintered at higher temperatures (a=8.3878(1)).

Ratios between X-ray diffraction lines (I_{220}/I_{440}) and (I_{440}/I_{422}) are closely related to the distributions of divalent, trivalent and tetravalent cations on octahedral and tetrahedral sites in spinel structures [33]. The relative integrated density (I_{hkl}) was calculated as [34]:

$$I_{hkl} = |F_{hkl}|^2 P L_p \quad (1)$$

where F_{hkl} is the structure factor, P is the multiplicity factor for the (hkl) plane and L_p is the Lorentz polarization factor determined as:

$$L_p = (1+\cos^2\theta)/(\sin^2\theta\cos\theta) \quad (2)$$

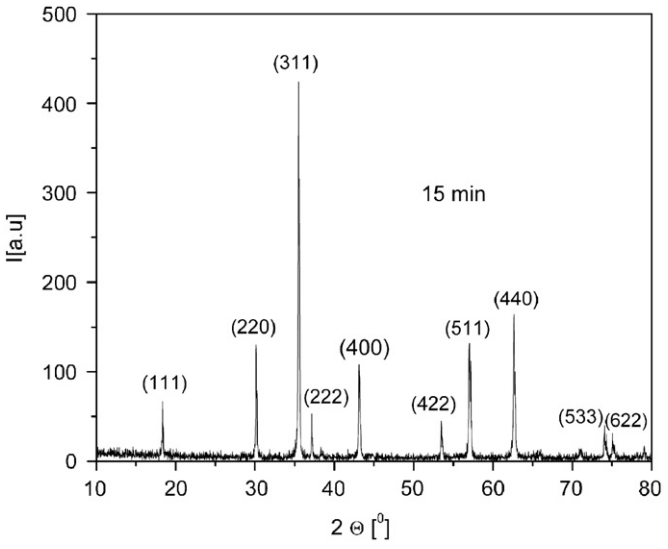

Fig. 1. XRD spectrum obtained for nickel manganite sample NMO-1200–15.

Table 1
The value of lattice constant for $NiMn_2O_4$ samples NMO-1200-(0–60) determined from Le-Bail full pattern profile fitting.

Activation time [min]	0	5	15	30	45	60
Parameter *a*	8.3970(2)	8.3899(2)	8.3914(6)	8.3903(7)	8.3955(7)	8.3884(2)

Variation of X-ray intensity ratios (I_{220}/I_{440}) and (I_{440}/I_{422}) calculated for $NiMn_2O_4$ samples using values determined from Le Bail full pattern profile fitting of XRD data is shown in Fig. 2. One can see that the intensity ratios vary depending on the time of mechanical activation of the starting powder in the manner that an increase of I_{220}/I_{440} corresponds to a decrease of I_{440}/I_{422}.

It was shown [34] that the intensity of the peaks is affected by the cation distribution in the AB_2O_4 spinel. When more heavy ions enter the A-site, the intensity ratio I_{220}/I_{440} increases, while I_{440}/I_{422} decreases which is case in $NiMn_2O_4$, when Mn^{2+} (0.81 Å) enter A site instead of Ni^{2+} (0.63 Å) because of Ni^{2+} displacement from tetrahedral to octahedral intersticies.

It was shown that the density of sintered samples changes with time of mechanical activation but more so with increasing sintering temperature [28]. One can note that the sample density increased for higher sintering temperatures. It also increased for shorter times of mechanical activation, reaching a maximum for about 30 min of mechanical activation times and then decreased for longer times of mechanical activation that is a consequence of powder agglomeration [29,32]. The changes in sample density are reflected in measured FIR reflection spectra in accordance with our previous analysis of $NiMn_2O_4$ sintered at different temperatures [31]. Fig. 3a shows changes in measured reflectivity spectra for $NiMn_2O_4$ samples activated for different times and sintered at 1200 °C, while Fig. 3b shows the measured reflectivity for a sample whose starting powder was activated for 5 min and then sintered at different temperatures.

Observed reflectivity spectra for analyzed samples showed the presence of the oscillators at the same wave number position, and reflectivity drop at 700 cm^{-1} as a consequence of a plasma effect. Intensities of peaks differ with time of mechanical activation and for different sintering temperatures. Evidently, the peaks at lower sintering temperatures are broader.This behavior is in correlation with microstructure changes during sintering and mechanical activation given in Fig. 4. During sintering microstructure changes are obvious and the sintering process goes through several stages. At 900 °C the sintering process has just started, at 1050 °C the process of neck forming has began, there are a lot of open pores and finally at 1200 °C the process approaches the final stage of sintering and closed pores can be noticed.

One can note that besides the influence of the sintering temperature that has been previously investigated [31], mechanical activation of starting powders also has an effect on the microstructure of sintered samples and prolonged milling time leads to agglomeration [32]. SEM studies of sintered

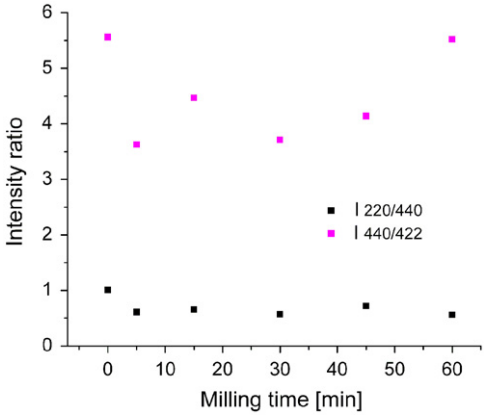

Fig. 2. X-ray intensity ratios (I_{220}/I_{440}) and I_{440}/I_{422}) vs time of mechanical activation.

nickel manganite samples revealed a strong influence of milling time on ceramic sample density. Longer mechanical activation (60 min) resulted in higher agglomeration and porosity (Fig. 5) which is later reflected in the intensity of IR reflection peaks. For each sintering temperature reflection spectra are similar for different times of mechanical activation with the exception of samples mechanically activated for 60 min which shows the lowest reflection due to the highest agglomeration degree.

The measured spectra for $NiMn_2O_4$ samples sintered at 1200 °C were analyzed using the four-parameter model of coupled oscillators introduced by Gervais and Piriou [35], where the factorized form of the dielectric function is defined as:

$$\varepsilon = \varepsilon_1 + i\varepsilon_2 = \varepsilon_\infty \prod_J \frac{\omega_{jLO}^2 - \omega^2 + i\gamma_{jLO}\omega}{\omega_{jTO}^{2-\omega^2} + i\gamma_{jTO}\omega} \quad (1)$$

where ω_{jLO} and ω_{jTO} are longitudinal (LO) and transversal (TO) frequencies, respectively, while γ_{jLO} and γ_{jTO} are their damping factors and ε_∞ is the high frequency dielectric permittivity. Good agreement between experimental and calculated diagrams was obtained. Six vibration modes were determined for all samples and the values of all calculated optical parameters are given in Table 2. Analysis of the reflectivity diagrams and calculated parameters from Table 2 shows that there are four strong ionic oscillators and two shoulders (at around 250 cm^{-1} and 530 cm^{-1}). Group theory predicts four active infrared modes for a normal spinel structure [36]. However, defects and disorder in the crystal lattice can be the reason for the higher number of calculated modes compared to the theoretically predicted number [37].

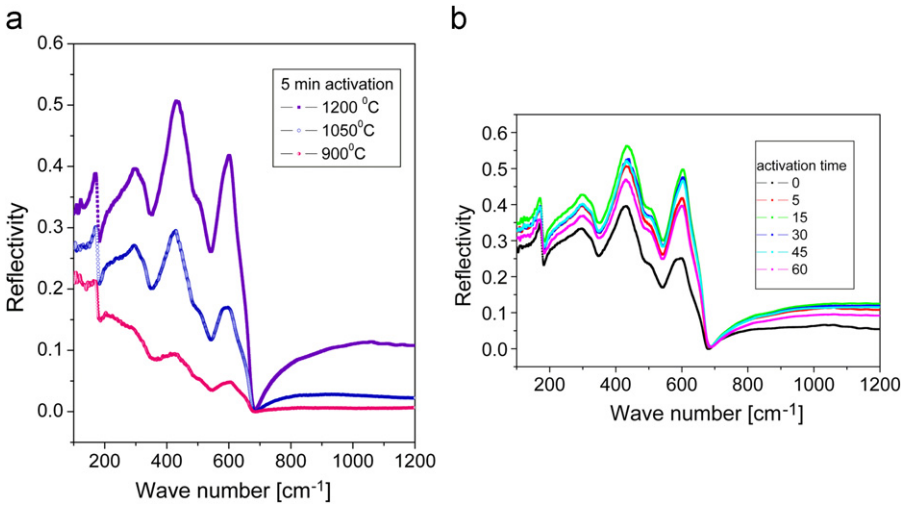

Fig. 3. (a) Reflectivity spectra for nickel manganite samples mechanically activated for 5 min and sintered at different temperatures and (b) IR reflectivity spectra for nickel manganite samples sintered at 1200 °C mechanically activated for different time.

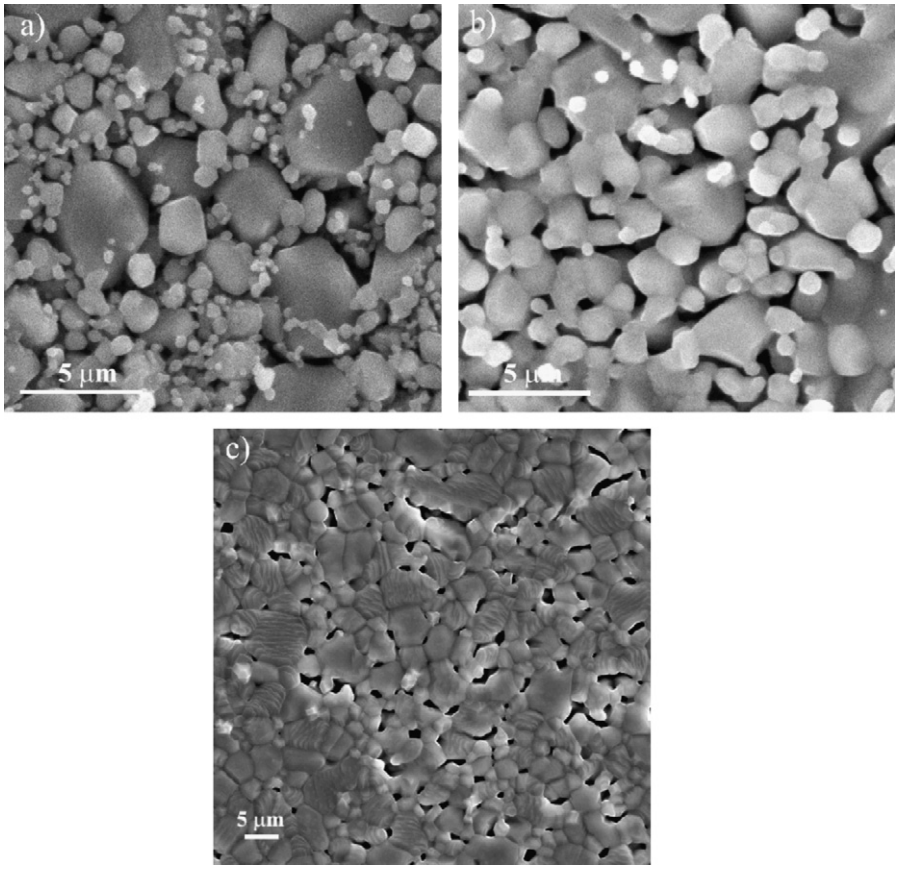

Fig. 4. Scanning electron micrographs of nickel manganite samples mechanically activated for 15 min and sintered at 900 °C (a), 1050 °C (b) and 1200 °C (c).

Thus, the four strong modes determined are in agreement with the number predicted from group theory, while the two shoulders can be an indication of a partially inverse spinel structure combined with defects due to mechanical activation.

As for assigning modes to certain groups, it is considered that for normal spinel structures the two high frequency modes can be assigned as vibrations of octahedral groups and the two low frequency modes are associated with vibrations of both octahedral and tetrahedral groups [38]. Such a claim does not stand when it comes to inverse spinels and assignment of only the highest frequency is taken as mixed vibrations of trivalent cations on both sites (octahedral and

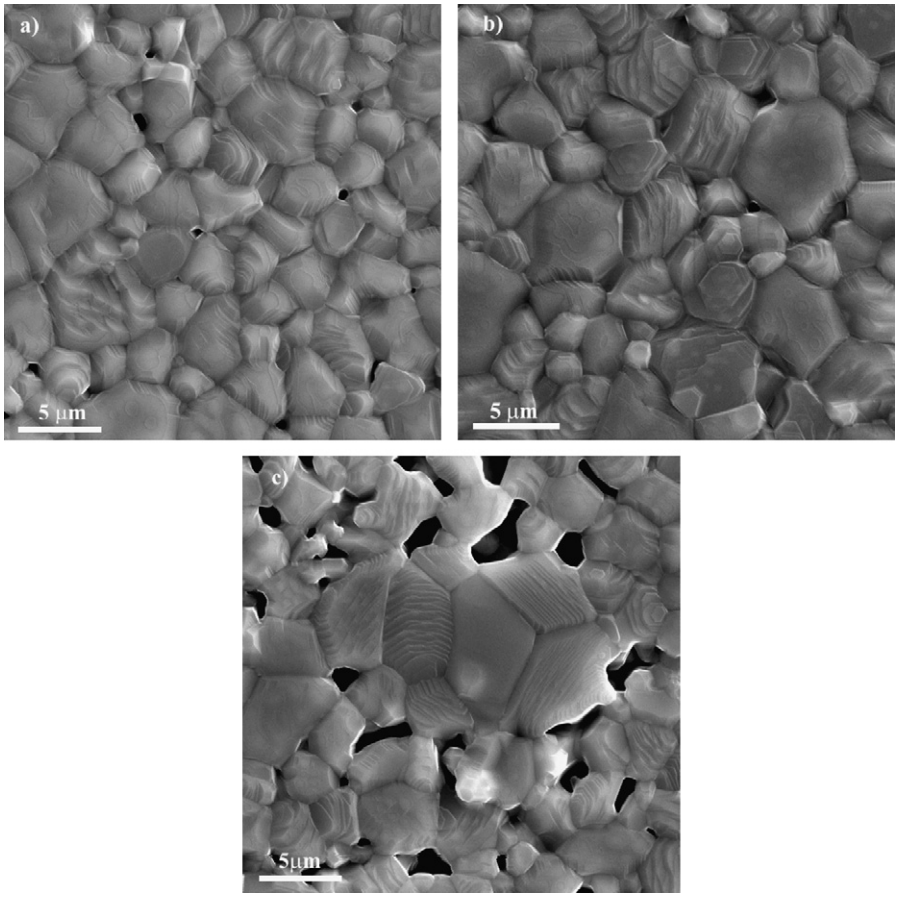

Fig. 5. Microstructures of the samples NMO-1200–30 (a), NMO1200–45 (b) and NMO-1200–60 (c).

Table 2
Transversal and longitudinal modes of and their corresponding damping factors (given in cm^{-1}) calculated for nickel manganite samples NMO-1200-(0–60).

Osc.	Activation time parameters	0	5	15	30	45	60
I	ω_{TO1}	174.5	174.5	174.5	174.5	174.5	174.5
	γ_{TO1}	12.9	11.9	11.9	11.8	13.4	16.0
	ω_{LO1}	178.1	178.1	178.1	178.1	178.1	178.1
	γ_{LO1}	10.9	10.7	11.0	10.9	12.6	13.8
II	ω_{TO2}	250.1	249.0	249.0	220.1	248.5	218.3
	γ_{TO2}	305.4	208.8	231.2	311.5	235.9	272.7
	ω_{LO2}	274.4	270.6	264.9	237.3	280.0	247.3
	γ_{LO2}	350.1	243.9	257.6	385.6	332.6	399.8
III	ω_{TO3}	310.8	318.3	316.6	319.2	324.8	319.1
	γ_{TO3}	111.8	66.6	63.8	63.9	58.8	58.8
	ω_{LO3}	344.9	337.5	336.4	337.0	336.8	332.9
	γ_{LO3}	89.7	63.2	61.3	59.4	53.4	57.0
IV	ω_{TO4}	414.5	419.3	422.0	423.9	422.5	422.9
	γ_{TO4}	73.0	57.8	53.2	51.0	58.0	56.9
	ω_{LO4}	483.2	477.6	479.1	468.4	463.1	461.9
	γ_{LO4}	88.1	111.8	89.1	99.7	96.4	93.6
V	ω_{TO5}	507.6	535.0	523.3	534.3	533.3	531.3
	γ_{TO5}	51.7	61.6	75.3	99.8	88.5	75.9
	ω_{LO5}	520.5	537.1	538.9	541.7	537.9	534.9
	γ_{LO5}	55.1	36.5	45.0	45.6	43.9	40.3
VI	ω_{TO6}	574.1	571.2	571.5	568.9	567.8	568.9
	γ_{TO6}	74.5	77.0	57.3	59.7	74.5	85.1
	ω_{LO6}	641.0	657.5	661.8	662.6	659.5	659.7
	γ_{LO6}	91.0	59.4	53.8	52.5	61.6	60.8
	ε_∞	3.43	5.01	5.62	5.19	4.37	4.28

Table 3
Born effective charges determined for NMO-1200-(0-60) samples.

Sample	Z_O	Z_{Ni}	Z_{Mn}
NMO-1200–0	1.90	1.83	2.88
NMO-1200–5	1.88	1.94	2.79
NMO-1200–15	1.92	1.92	2.92
NMO-1200–30	1.87	1.91	2.78
NMO-1200–45	1.85	1.76	2.82
NMO-1200–60	1.83	1.94	2.62

tetrahedral). Finally, in the case of intermediate $NiMn_2O_4$ structure all determined ionic oscillators originate from the vibrations of all atoms and forces in the lattice [31].

Born effective charges can be calculated from TO/LO splittings of the phonon modes using the relation [39]:

$$\sum_{j=1}^{n_{IR}} (\omega_{jLO}^2 - \omega_{jTO}^2)_a = \frac{1}{\varepsilon_0 V} \sum_{k=1}^{n_{atom}} \frac{Z_{ka}^2 e^2}{m_k} \quad (2)$$

where a is the polarization direction, the summation on the right-side of the equation is over all atoms in the unit cell and the summation on the left-hand side is over all active IR-modes, ε_0 is the vacuum dielectric constant, V is the unit cell volume, m_k is the atomic mass and e is the electron charge. The charge neutrality condition also needs to be satisfied and in the case of $NiMn_2O_4$ it is:

$$Z_{Ni} + 2Z_{Mn} + 4Z_O = 0 \quad (3)$$

where Z_{Ni}, Z_{Mn} and Z_O are the Born effective charges of Ni, Mn and O atoms. In the ideal case these charges would be +2 for Ni, +3 for Mn and −2 for O atoms. The values calculated for samples NMO-1200-(0-60) are given in Table 3.

All obtained values for Born effective charges are lower than the formal charges of Ni and Mn cations, indicating some hybridization between the cations and O anions due to structural disorder and defects.

4. Conclusion

Obtained IR spectra for all analyzed samples showed the presence of the same oscillators (four strong and two shoulders) but their intensities increased with the sintering temperature in correlation with the increase in sample density and microstructure development during sintering. Besides the applied sintering temperature, mechanical activation of starting powders also has an effect on the measured reflectivity spectra where higher peak intensities were measured for the activated samples that had a higher density while nonactivated (most porous) samples had the lowest intensities.

SEM studies of sintered nickel manganite samples revealed the strong influence of milling time on ceramic density. Longer mechanical activation (60 min.) resulted in higher agglomeration and porosity that clearly reflected in the intensity of IR reflection peaks.

Acknowledgements

The Ministry of Science and Education of the Republic of Serbia supported this work (Project no. III45007).

References

[1] E.D. Macklen, Thermistors, Electrochemical Publications, Glasgow, 1979.
[2] H.B. Sahse, Semiconducting Temperature Sensors and Their Applications, Wiley, New York, 1975.
[3] L. Edwards, R. Murthy, Versatile thermistors for wide-ranging applications, Electrotechnology 15 (1987) 89–91.
[4] M.L. Singla, S. Sharma, B. Raj, V.R. Harchekar, Characterization of transition metal oxide ceramic material for continuous thermocouple and its use as NTC fire wire sensor, Sensors and Actuators A: Physical 120 (2005) 337–342.
[5] S. Karanth, M.A. Sumesh, V. Shobha, H. Ganesh Shanbhogue, C.L. Nagendra, Infrared detectors based on thin film thermistor of ternary Mn–Ni–Co–O on micro-machined thermal isolation structure, Sensors and Actuators A: Physical. 153 (2009) 69–57.
[6] P. Umadevi, C.L. Nagendra, Preparation and characterisation of transition metal oxide micro-thermistors and their application to immersed thermistor bolometer infrared detectors, Sensors and Actuators A: Physical 96 (2002) 114–124.
[7] O.S. Aleksić, S.M. Savić, M.D. Luković, K.T. Radulivić, V.Z. Pejović, Segmented thermistors printed by NTC nanometric paste and applied in volume air-flow sensors, Materials Science Forum 518 (2006) 247–252.
[8] O.S. Aleksić, S.M. Savić, M.V. Nikolić, L. Sibinoski, M.D. Luković, Micro-flow sensors for water using NTC thick film segmented thermistors, Microelectronics International 26 (3) (2009) 30–34.
[9] M.V. Nikolić, B.M. Radojčić, O.S. Aleksić, M.D. Luković, P.M. Nikolić, A thermal sensor for water using self-heated NTC thick-film segmented thermistors, IEEE Sensors Journal 11 (8) (2011) 1640–1645.
[10] N.P. Parasanth, J.M. Varghese, K. Prasad, B. Krishnan, A. Seema, K.R. Dayas, Tape casting of nickel manganite NTC ceramics for chip thermistors, Journal of Materials Science - Materials in Electronics 19 (2008) 1100–1104.
[11] R. Metz, Electrical properties of N.T.C. thermistors made of manganite ceramics of general spinel structure: $Mn_{3-x-x'}M_xN_{x'}O_4$ ($0 \le x+x' \le 1$; M and N being Ni, Co or Cu). Aging phenomenon study, Journal of Materials Science 35 (2000) 4705–4711.
[12] A. Díez, R. Schmidt, A.E. Sagua, M.A. Frechero, E. Matesanz, C. Leon, E. Morán, Structure and physical properties of nickel manganite $NiMn_2O_4$ obtained from nickel permanganate precursor, Journal of the European Ceramic Society 30 (2010) 2617–2624.
[13] N.J. Podraza, D.B. Saint John, S.W. Ko, H.M. Schulze, J. Li, E.C. Dickey, S. Trolier-McKinstry, Optical and structural properties of solution deposited nickel manganite thin films, Thin Solid Films 519 (2010) 2919–2923.
[14] S.W. Ko, J. Li, N.J. Podraza, E.C. Dickey, S. Trolier-McKinstry, Spin spray-deposited nickel manganite thermistor films for microbolometer applications, Journal of the American Ceramic Society 94 (2) (2011) 516–523.
[15] D.-L. Fang, Z.-B. Wang, P.-H. Yang, W. Liu, C.-S. Chen, A.J.A. Winnubst, Preparation of ultra-fine nickel manganite powders and ceramics by a solid-state coordination reaction, Journal of the American Ceramic Society 89 (1) (2006) 230–235.
[16] H. Schulze, J. Li, E.C. Dickey, S. Trolier-McKinstry, Synthesis, phase characterization, and properties of chemical solution-deposited nickel manganite thermistor thin films, Journal of the American Ceramic Society 92 (3) (2009) 738–744.
[17] C.-H. Zheng, D.-L. Fang, Preparation of ultra-fine cobalt–nickel manganite powders, and ceramics derived from mixed oxalate, Materials Research Bulletin 43 (2008) 1877-1872.

[18] C. Zhao, B. Wang, P. Yang, L. Winnubst, C. Chen, Effects of Cu and Zn co-doping on the electrical properties of Ni0.5Mn2.5O4 NTC ceramics, Journal of the European Ceramic Society 28 (2008) 35–40.
[19] J.A. Schmidt, A.E. Sagua, J.C. Bazán, M.R. Prat, M.E Braganza, E Morán, Nickel Permanganate as a precursor in the synthesis of a $NiMn_2O_4$ spinel, Materials Research Bulletin 40 (2005) 635–642.
[20] J.M. Varghese, A. Seema, K.R. Dayas, Ni–Mn–Fe–Cr–O negative temperature coefficient thermistor compositions: correlation between processing conditions and electrical characteristics, Journal of Electroceramics 22 (2009) 436–441.
[21] K. Park, Fabrication and electrical properties of Mn–Ni–Co–Cu–Si oxides negative temperature coefficient thermistors, Journal of the American Ceramic Society 88 (4) (2005) 862–866.
[22] P.N. Lisboa-Filho, L.A. Baring, L. Walmsley, M. Bahout, P. Barahona, O. Peña, C. Moure, Metal–insulator transitions and magnetic ordered states in oxygen–depleted manganites, Physica B 378–380 (2006) 522–524.
[23] P.N. Lisboa-Filhoa, M. Bahouta, P. Barahonaa, C. Mourec, O. Peña, Oxygen stoichiometry effects in spinel-type $NiMn_2O_{4-\delta}$ samples, Journal of Physics and Chemistry of Solids 66 (2005) 1206–1212.
[24] O. Peña, X. Cailleaux, B. Piriou, M. del Canto, S. Abarca, E. Ríos, J. Ortiz, J.L. Gautier, P.N. Lisboa-Filho, C. Moure, Magnetic properties of $Cu_{1+x}Mn_{2-x}O_4$ and $Ni_{1+x}Mn_{2-x}O_4$ solid solutions, Journal of the European Ceramic Society 27 (2007) 3911–3914.
[25] O. Peña, C. Moure, V. Bodenez, X. Cailleaux, B. Piriou, J. Ortiz, G. Zuñiga, J.L. Gautier, P.N. Lisboa-Filho, Magnetic properties of spinel-type oxides $NiMn_{2-x}Me_xO_4$, Journal of the Chilean Chemical Society 50 (3) (2005) 617–623.
[26] P. Barahona, V. Bodenez, T. Guizouarn, O. Peña, J. Ortiz, E. Rios, R. Pastene, J.L. Gautier, Substitution effects on the magnetic properties of $Ni(Me,Mn)_2O_4$ and $Li(Me,Mn)_2O_4$: comparison between Me=Cr and Fe, Journal of the Chilean Chemical Society 50 (2) (2005) 495–499.
[27] S.M. Savić, O.S. Aleksić, M.V. Nikolić, D.T. Luković, V.Ž. Pejović, P.M. Nikolić, Thermal diffusivity and electron transport properties of NTC samples obtained by the photoacoustic method, Materials Science and Engineering: B Advanced 131 (2006) 216–221.
[28] S.M. Savić, M.V. Nikolić, O.S. Aleksić, M. Slankamenac, M. Živanov, P.M. Nikolić, Intrinsic resistivity of sintered nickel manganite vs. powder activation time and density, Science of Sintering 40 (1) (2008) 27–32.
[29] S.M. Savić, G.M. Stojanović, M.V. Nikolić, O.S. Aleksić, D.T. Luković Golić, P.M. Nikolić, Electrical and transport properties of nickel manganite obtained by Hall effect measurements, Journal of Materials Science - Materials in Electronics 20 (2009) 242–247.
[30] M.V. Nikolic, S.M. Savic, O.S. Aleksic, K.M. Paraskevopoulos, T.T. Zorba, V. Blagojevic, P.M. Nikolic, Changes of structural, optical and electrical properties of nickel-manganite ceramics induced by additional mechanical activation, Proc. 10th ECerS Conf., Göller Verlag, Baden-Baden, 2007, 809–813.
[31] M.V. Nikolić, K.M. Paraskevopoulos, O.S. Aleksić, T.T. Zorba, S.M. Savić, V.D. Blagojević, D.T. Luković, P.M. Nikolić, Far infrared reflectance of sintered nickel manganite samples for negative temperature coefficient thermistors, Materials Research Bulletin 42 (2007) 1492–1498.
[32] S.M. Savić, L. Mančić, K. Vojisavljević, G. Stojanović, Z. Branković, O.S. Aleksić, G. Brankovic, Microstructural and electrical changes in nickel manganite powder induced by mechanical activation, Materials Research Bulletin 46 (2011) 1065–1071.
[33] Z. Wang, C. Zhao, P. Yang, A.J.A. Winnubst, C. Chen, X-ray diffraction and infrared spectra studies of $Fe_xMn_{2.34-x}Ni_{0.66}O_4$ ($0 < x < 1$) NTC ceramics, Journal of the European Ceramic Society 26 (2006) 2833–2837.
[34] D.S. Birajdar, U.N. Devatwal, K.M. Jadhav, X-ray, IR and bulk magnetic properties of $Cu_{1+x}Mn_xFe_{2-2x}O_4$ ferrite system, Journal of Materials Science 37 (2002) 1443–1448.
[35] F. Gervais, B. Piriou, Temperature dependence of transverse- and longitudinal-optic modes in TiO_2 (rutile), Physical Review B 10 (1974) 1642–1654.
[36] D.M. Adams, D.C. Newton, Tables for Factor Group and Point Group Analysis, Beckman MIIC, Croydon, UK, 1970.
[37] M.V. Nikolić, N. Obradović, K.M. Paraskevopoulos, T.T. Zorba, S.M. Savić, M.M. Ristic, Far infrared reflectance of sintered Zn_2TiO_4, Journal of Materials Science 43 (2008) 5564–5568.
[38] M. Lenglet, F. Hochu, Correlation between ionic-covalent parameters and infrared spectroscopic data in II-III transition metal spinel-type oxides, Materials Research Bulletin 32 (1997) 863–872.
[39] T. Kurosawa, Polarization waves in solids, Journal of the Physical Society of Japan 16 (1961) 1298–1308.